catalysts

MDPI

Article

Enhanced Oil Recovery by In-Reservoir Hydrogenation of Carbon Dioxide Using Na-Fe_3O_4

Firdavs Aliev [1,*], Temurali Kholmurodov [1,2], Oybek Mirzayev [1], Arash Tajik [1], Nurali Mukhamadiev [2], Olga Slavkina [3], Nuriya Nourgalieva [1] and Alexey Vakhin [1,*]

[1] Institute of Geology and Petroleum Technologies, Kazan Federal University, 420008 Kazan, Russia
[2] Department of Chemistry, Samarkand State University, Samarkand 140104, Uzbekistan
[3] RITEK LLC, 400048 Volgograd, Russia
* Correspondence: aquathermolysis@gmail.com (F.A.); vahin-a_v@mail.ru (A.V.)

Abstract: In-situ conversion of carbon dioxide into value-added products is an essential process in terms of heavy oil upgrading and utilization of the main anthropogenic greenhouse gas. In this paper, we discuss a synthesis of sodium-coated magnetite (Fe_3O_4) particles for in-reservoir hydrogenation of CO_2. The performance of the obtained catalyst was tested in upgrading of heavy oil in a High Pressure/High Temperature (HPHT) reactor imitating the reservoir conditions during steam injection techniques. The experiments were conducted for 48 h in a CO_2 environment under the steam temperature and pressure of 250 °C and 90 bar, respectively. The results showed irreversible viscosity reduction of oil from 3931 mPa·s to 2432 mPa·s after the degassing of unreacted carbon dioxide. The content of resins in the composition of upgraded oil was significantly altered from 32.1 wt% to 19.01 wt%, while the content of aromatics rose from 32.5 wt% to 48.85 wt%. The GC-MS results show the presence of alkyl benzenes and phenanthrenes, which were initially concentrated in resins and asphaltenes, in the aromatics fraction of upgraded crude oil. Thus, Na-Fe_3O_4 exhibits promising results for in-situ heavy oil upgrading through the hydrogenation of carbon dioxide, which contributes not only to the reduction of greenhouse gas emissions, but also enhances heavy oil recovery.

Keywords: heavy oil; steam; EOR; CO_2; hydrogenation; catalysts; carbon dioxide utilization; in-situ upgrading

Citation: Aliev, F.; Kholmurodov, T.; Mirzayev, O.; Tajik, A.; Mukhamadiev, N.; Slavkina, O.; Nourgalieva, N.; Vakhin, A. Enhanced Oil Recovery by In-Reservoir Hydrogenation of Carbon Dioxide Using Na-Fe_3O_4. *Catalysts* **2023**, *13*, 153. https://doi.org/10.3390/catal13010153

Academic Editor: Zhong-Wen Liu

Received: 7 December 2022
Revised: 30 December 2022
Accepted: 4 January 2023
Published: 9 January 2023

1. Introduction

The dramatic increase of anthropogenic greenhouse gas emissions into the atmosphere was noticed after the boom of industrialization. An increase in carbon dioxide emissions from industrial enterprises leads to an increase in the global temperature of the planet, and, consequently, we face global warming and climate change. The world carbon dioxide emissions are expected to rise up to 43.08 billion metric tons by 2050, in contrast to 35.3 billion metric tons of carbon dioxide, which was estimated in 2018 [1,2]. This requires the development and implementation of new and efficient technologies to reduce the concentration of carbon dioxide in the earth's atmosphere, in particular through the use of various chemical processes in which CO_2 acts as the main reactant. The inertness of the CO_2 molecule is the biggest challenge to the implementation of such processes [3]. One of the promising methods for utilizing CO_2 is hydrogenation of CO_2 in the presence of a catalyst. From this point of view, carbon dioxide can be considered as an attractive renewable source for obtaining more valuable organic compounds. In recent years, the conversion of CO_2 into value-added products has been widely studied due to their practical significance not only in terms of catalysis and environmental issues, but also in terms of upgrading heavy oil and enhancing oil recovery. The hydrogenation of carbon dioxide, depending on the reaction conditions and nature of catalysts, can yield methanol, formic acid, olefins, and

n-alkanes [4–6]. These products are significant for the partial upgrading of heavy crude oil, which suffers from a high content of resins and asphaltenes, low H/C ratio, and high content of heteroatoms and metals [7,8]. Although the estimated reserves of heavy oil are huge (70% of world's total oil reserves) [9], all these challenges make the heavy crude oil immobile in reservoir conditions, hard to recover, and hard to process. Thermal-enhanced oil recovery (mainly steam-based technologies) techniques are widely applied industrial methods to unlock potential heavy oil and natural bitumen reserves. However, the drawbacks of steam injection techniques are high energy costs and huge freshwater resources required to generate steam [10]. Moreover, burning fuels leads to environmental pollution by producing CO_2 [11]. It was reported that viscosity regression of heavy oil occurs on the surface due to the polymerization of hydrocracked fragments such as free radicals [12]. Therefore, co-injection of carbon dioxide with steam is considered as an alternative new emerging method to improve the efficiency of the steam recovery method through hydrogenation of carbon dioxide in place [13–15]. Moreover, the unreacted carbon dioxide in supercritical conditions acts as an excellent viscosity-reducing substance, which has high solubility and miscibility with crude oil [16,17]. Recently, the selective hydrogenation of carbon dioxide into methane, methanol, dimethyl ether, olefins, aromatics, and higher alcohols has been extensively studied [18–20]. Homogeneous and heterogeneous catalysts for the hydrogenation of CO_2 are widely applied in order to improve the kinetics of the reaction and the selectivity of product formation. Generally, homogeneous catalysts exhibit high activity and selectivity in hydrogenation reactions, but it is difficult to isolate them from the reaction products and regenerate them. At the same time, heterogeneous catalysts are more thermally stable, cheaper, and easier to use, which makes them promising for large-scale industrial applications [21,22]. Although the hydrogenation of CO_2 on heterogeneous catalysts in order to obtain valuable products remains a serious problem due to the high energy barrier of the C-C bond and the competition of the formation of C-C bonds with the formation of H-H and C-H bonds, significant progress has been made in this direction in recent years [23,24]. Based on the nature of the catalysts and the conditions of the process, various chemicals can be obtained by hydrogenation of CO_2, such as C2–C4 alkanes and higher alkanes (C5+), light olefins C2–C4, and other substances, which can be either an intermediate stage of hydrocarbon synthesis or raw materials for other downhole chemical reactions [25]. These products are primarily carbon monoxide, methane, and methanol [26].

The Reaction (1) of CO_2 conversion into CO is the reverse reaction of water gas shift (RWGS). This reaction is one of the most researched areas in the field of carbon dioxide processing. It occurs in any system where carbon dioxide and hydrogen are present.

$$CO_2 + H_2 \rightarrow CO + H_2O,\ \Delta H_{298} = 41.2\ \text{kJ/mol} \quad (1)$$

This reaction is endothermic; hence an increase in temperature may shift the equilibrium towards the formation of CO. The low value of the equilibrium constant is the main obstacle to the conduction of the RWGS reaction. Some of the most popular catalysts applied in RWGS: Cu/ZnO catalysts modified by titanium, zirconium, and aluminum oxide [27]; and modified commercial catalysts based on iron with catalytic additive—Cr_2O_3. The thermal stability of the iron-based catalysts is above 400 °C [28]. Moreover, these catalysts are less poisoned by chlorine, alkalis, and sulfur-containing compounds [29].

The alternative reaction path (2) for the hydrogenation of carbon dioxide was proposed by Sabatier [30]:

$$CO_2 + 3H_2 \rightarrow CH_4 + H_2O,\ \Delta H_{298} = -259.9\ \text{kJ/mol} \quad (2)$$

Although the formation of methane is easier from the thermodynamic point of view, the active catalyst is required to enhance the kinetic parameters of the process. In the literature, the thermodynamics and kinetic parameters of the given reaction path are thoroughly discussed [31,32]. From the periodic table, d-elements of the VIII group, particularly Ni, Fe, Ru, Rh, and Co, are reported as promoters of carbon dioxide methanation [33–35]. However,

nickel-based catalysts are considered active and with high selectivity to methane formation. The deterministic factor of nickel activity is an interaction of nickel with the catalyst carrier. Nakayama et al. synthesized and demonstrated the catalytic activity of Ni/MgO on carbon dioxide methanation [36]. Du et al. imply that the Ni- incorporated MCM-41 catalyst provides up to 96% selectivity to methane formation [37]. Attention is paid to Raney nickel, which also exhibits excellent catalytic properties [38]. Such performance can be attributed to its unique thermal and structural properties, as well as its large specific surface area. An increase in the Ni content leads to a more selective formation of methane up to 100% [39]. It is well-known that iron-based catalysts are active in WGS reactions, especially in the production of hydrocarbons in the Fischer-Tropsch process [40,41]. However, there is little information on the effective formation of CH_4 during the hydrogenation of CO_2 using Fe-based catalysts. It is difficult to judge because of the wide range of products formed on these catalysts during the hydrogenation of carbon dioxide, including CO, CH_4, higher alkanes, olefins, and even alcohols. The effect of various promoters on the activity and selectivity of iron-containing catalysts in the hydrogenation of CO_2 was systematically investigated by several authors in order to increase the yield of products [40–42]. Fischer-Tropsch catalysts based on iron usually contain an additive of potassium, which increases the adsorption of carbon oxides CO_x while reducing the adsorption of hydrogen. Therefore, the yield of hydrocarbons and olefins increases with the addition of additives such as potassium and sodium [43]. Similar effects towards increasing the average molecular weight of hydrocarbon products were reported for copper-promoted precipitated iron-based catalysts [44–53].

The direct conversion of CO_2 into light *n*-alkanes can be considered as a modification of Fischer-Tropsch synthesis, where CO_2 is implemented instead of CO. Many authors tried to adapt Fischer-Tropsch catalysts for the maximum light *n*-alkane yield [41,47,53]. In a Fischer-Tropsch process, the competition between CO and CO_2 is an important aspect to be taken into account. Some authors show the results of H_2-CO, H_2-CO_2 and (CO + CO_2)-H_2 conversion over cobalt catalysts under typical Fischer-Tropsch process conditions [53,54]. They imply that the catalysts show similar identical activity, but different selectivity for the formation of products in the presence of only CO or CO_2 in mixtures with hydrogen. The CO hydrogenation led to the normal distribution of Fischer-Tropsch synthesis products with a chain growth probability of about 0.80. At the same time, the products of CO_2 hydrogenation at the same reaction condition contained more than 70% methane. Consequently, the routes of hydrogenation reactions of CO_2 and CO are different. Significant difference is also observed in terms of the stability of the catalysts. The catalysts in CO medium lose their activity faster than CO_2 medium. The different catalytic behavior can be explained by different rates of intermediate formation, suppression of methane and desorption of chain growth products. Many scholars mention the promotion of iron-based Fischer-Tropsch catalysts by Al_2O_3 carrier and K promoter. Iron oxides are attractive for the synthesis of hydrocarbons due to the formation of olefins [55]. The selectivity of iron-based nanoparticles to the production of CO_2 in the WGS reaction is very high, which is an unwanted product for the Fischer-Tropsch process. However, it can be favorable in terms of carbon dioxide hydrogenation into light *n*-alkanes. Two-step reaction path was proposed for the conversion of CO_2 on the surface of iron nanoparticles into *n*-alkanes. The first step is the conversion of CO_2 into CO via RWGS reaction. The second step is the conversion of unstable syngas into value-added *n*-alkanes.

The iron-based catalyst without promoters has a number of negative limitations in terms of stability, activity and selectivity for hydrocarbon products. In order to increase the yield of desired hydrocarbon products, promoters are often added to catalysts in order to adapt and optimize the distribution of products for a specific task. Usually, the nature of the catalyst is the main factor significantly affecting the selectivity and activity of the product. Although iron catalysts are able to convert CO_2 with a much greater selectivity for the formation of alkenes and long-chain hydrocarbons compared to other metals, the unalloyed catalyst still demonstrates a high selectivity with respect to undesirable

products, and therefore it is necessary to use promoters in order to achieve high yields of target products [56].

Alkaline elements such as Na and K enhance catalytic activity of the catalysts by promoting electronegativity to shift the distribution of products. Moreover, the transfer of electrons to the free orbital of metals can increase the basicity of the catalyst surface and hence, increase the CO_2 adsorption rather than hydrogen. Optimizing the content of promoters can increase the olefin/paraffin ratio and the average molecular weight of products [43]. Recently Na-modified Fe-Zn catalysts have been synthesized by hydrothermal method using microwave radiation using the Na-containing precursor $ZnFe_2O_4$. The $ZnFe_2O_4$ catalyst in the presence of Na with the concentration of 0.08%wt. demonstrated high activity in conversion of CO_2 into C5+ hydrocarbons in contrast to the Fe_2O_3 and mixed ZnO-Fe_2O_3 catalysts. The selectivity in the presence of sodium reached 58%, while the ratio of olefin-to-paraffin in the reaction products was 11. The literature review on the topic of carbon dioxide hydrogenation revealed a number of studies devoted to the catalysis of heterogeneous catalytic systems. Most of the scholars focused on the catalysis of downstream hydrogenation processes of carbon dioxide in facilities to increase the yield of value-added chemical products. To the best of our knowledge, there are few works on in-reservoir catalytic hydrogenation of carbon dioxide to enhance heavy oil upgrading and recovery. Thus, promoting in-situ hydrogenation of carbon dioxide with highly selective catalysts is not only a promising means of carbon dioxide utilization but also can be considered as an effective approach to modify steam-based heavy oil recovery methods [41,43,45–50].

In this paper, we synthesized Na-Fe_3O_4 nanoparticles to catalyze the in-situ hydrogenation of carbon dioxide. The nanoparticles were thoroughly characterized by analytical methods. The hydrogenation and upgrading performance of Na-Fe_3O_4 was evaluated by employing the structural, group, and elemental composition of the upgrading products. Moreover, the viscosity reduction degree in the presence of nanoparticles was evaluated.

2. Results and Discussions

The first part of the results is devoted to the characterization of the nanoparticles, which was thoroughly investigated by several analytical methods such as FT-IR, SEM, and XRD. In the second part of the study, the catalytic performance of the achieved catalysts on hydrogenation and upgrading of heavy oil samples was assessed.

2.1. Characterization of the Catalyst

2.1.1. FT-IR Analysis of the Achieved Catalysts

According to the synthesis procedure of Na-Fe_3O_4 nanoparticles, which is described in Section 3.1, the product of the first step reaction should yield magnetite (Fe_3O_4) (Figure 1), which further interacts with NaOH during the second step reaction. The reaction of magnetite with sodium hydroxide under 500–600 °C yields Na-Fe_3O_4, which was clearly observed in FT-IR spectroscopy of the product (Figure 1). The peaks around 1500 cm^{-1}, which correspond to the Fe_3O_4 and FeO were not detected in the specter of the end-product, while a peak around 800 cm^{-1} corresponds to Na-Fe_3O_4.

2.1.2. XRD

The XRD analysis method was employed to reveal the structural composition of the achieved catalyst particles (Figure 2). The results were in accordance with the FT-IR results and proved the synthesis of Na-Fe_3O_4. The XRD pattern illustrated in Figure 2, shows the characteristic spectrum lines of Na-Fe_3O_4 at degrees (2θ) of 20, 20.1, 29.6, 31.8, 33.3, 34.1, 35.7, 54.1, 58, 72, 76, 81 and 83 corresponding to the (125), (141), (160), (130), (413), (207), (337), (290), (137), (150), (110), (85) and (105) planes of the crystals, correspondingly. However, there was observed hematite with its amorphous structure, which reflects the intensity of the peaks. The elemental composition of the catalyst surface and

the relative content of elements in the composition of the catalyst was further analyzed by electronic microscope.

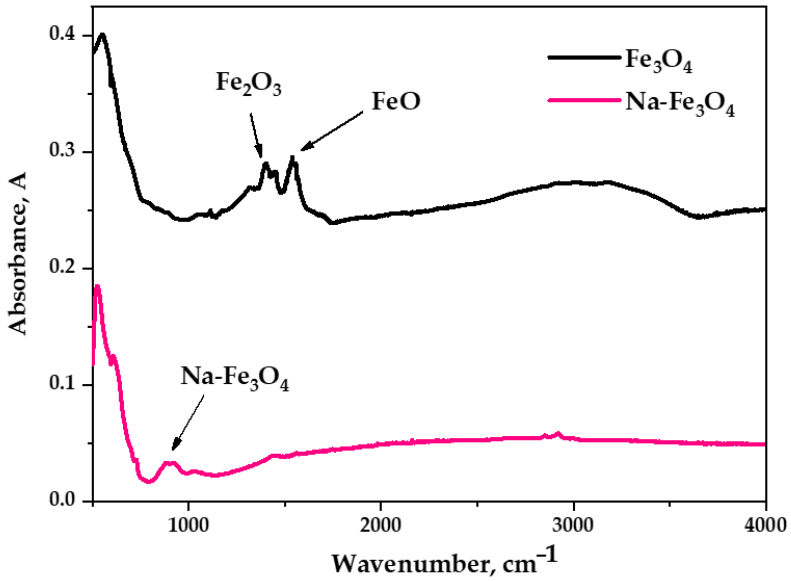

Figure 1. The FT-IR spectra of magnetite and Na-Fe_3O_4.

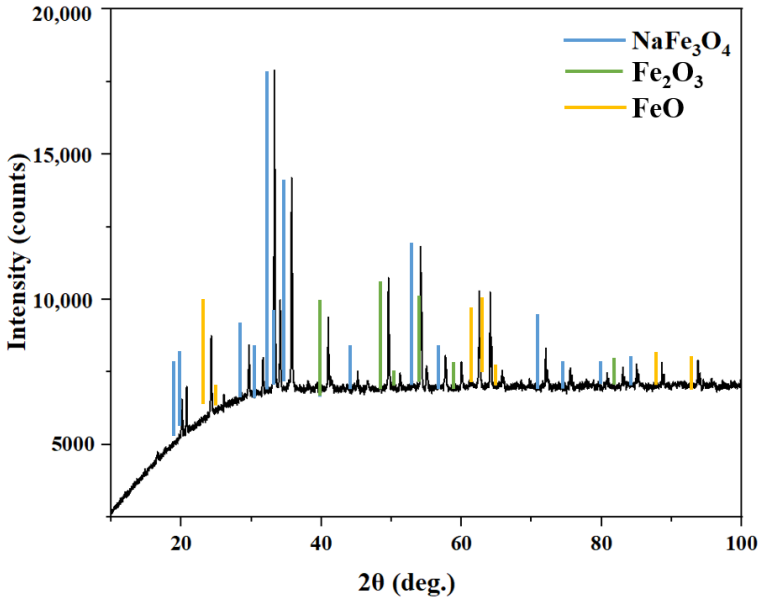

Figure 2. XRD pattern of the synthesized catalyst.

2.1.3. SEM and EDX

The particle size distribution of the catalysts is one of the crucial characteristics affecting the efficiency of the process. The surface area strongly depends on the size of the particles. Therefore, we scanned the achieved catalyst with an electronic microscope to reveal the particle size distribution of the catalyst, as well as the elemental distribution of the catalyst surface. In Figure 3, we present the SEM image of the Na-Fe_3O_4 catalyst particles. The particle size distribution with their relative frequency is provided by Figure 4. Although the particles with the size range of 101–141 nm are abundant (41%), the nanosized particles within the range of 20–100 have a frequency of more than 50%. The relative content of 20–60 nm particles is 17%, while the relatively large particles with the size range of 140–180 make only 5%.

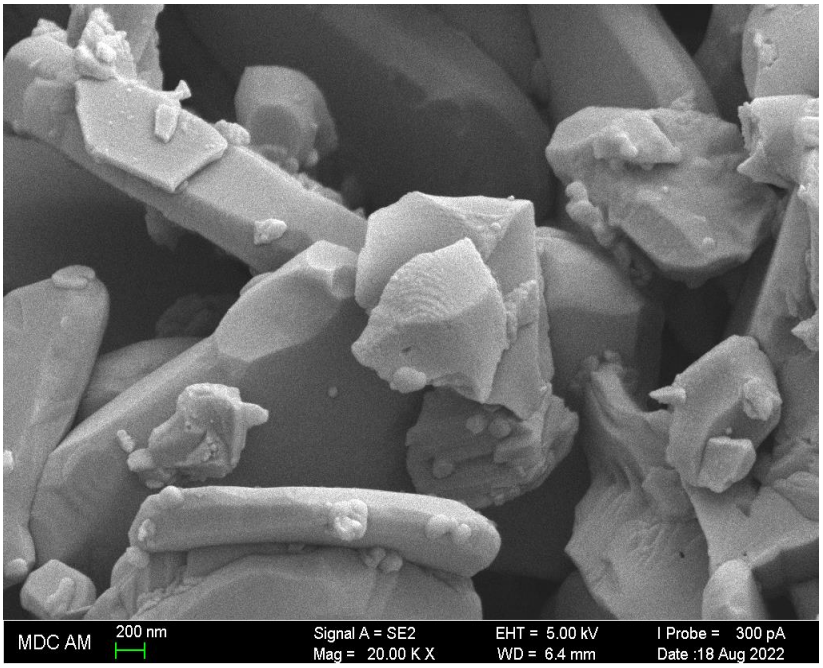

Figure 3. SEM image of the Na-Fe_3O_4 catalyst particles.

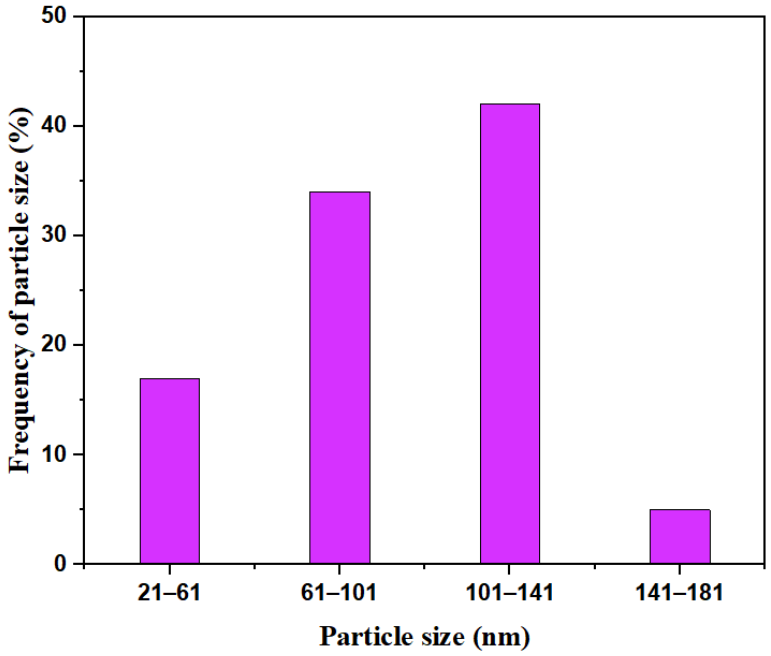

Figure 4. The particle size distribution of the obtained catalyst.

The elemental composition of the nanocatalysts observed from the specter (Figure 5a) of Energy Dispersive X-ray mapping is summarized in Table 1. The relative content of surface elements was estimated in the fragment illustrated in Figure 5b. It was observed that the content of iron and sodium elements predominated on the surface of the catalyst, which was manifested in the intensity of the corresponding peaks. According to the results, the structure of the obtained catalyst is mainly composed of iron-containing species and sodium (83.78 and 10.63, correspondingly), which indicates the magnetic crystalline structure of Na-Fe_3O_4.

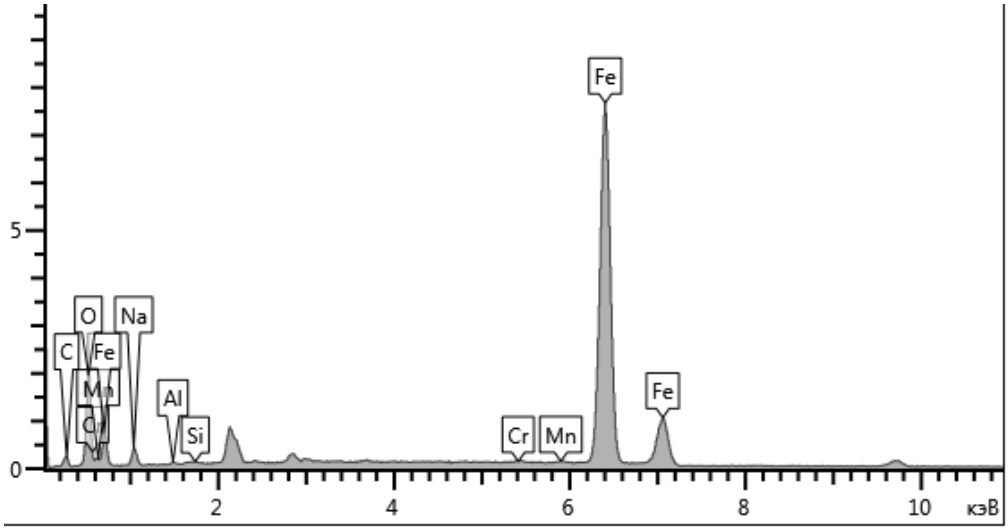

(**a**)

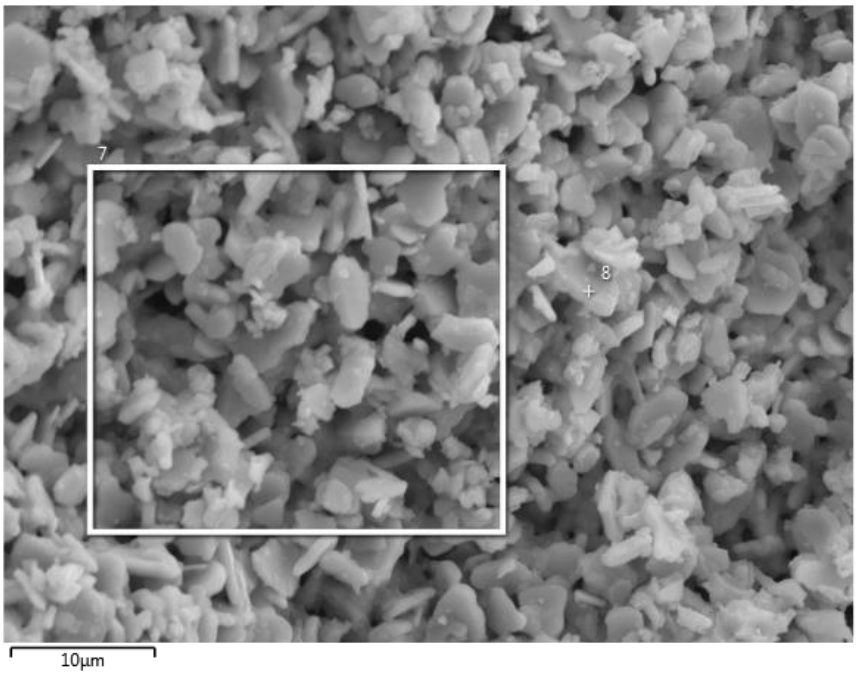

(**b**)

Figure 5. Elemental distribution (**a**) of the obtained catalyst nanoparticles surface and image (**b**) of surface fragment.

Table 1. The mass and atomic content of elements.

Elements	Relative Content (wt.%)	Relative Content (Atom.%)
O	4.82	16.11
Na	10.63	21.44
Al	0.17	0.26
Si	0.12	0.17
Cr	0.16	0.13
Mn	0.32	0.25
Fe	83.78	61.64
Sum	100	100

2.2. Upgrading Performance of the Synthesized Catalyst Nanoparticles

The obtained catalyst was used to upgrade a heavy oil sample by promoting the hydrogenation of CO_2 during steam injection processes. For this purpose, the autoclave experiments were carried out to imitate the in-situ CO_2-assisted hydrothermal upgrading of heavy oil at 250 °C in the absence and presence of the obtained catalyst. The hydrogenation and upgrading performances were evaluated using several analytical methods such as GC of the evolved gasses, FT-IR spectroscopy of the crude oil sample before and after the catalytic treatment, EPR analysis, CHNS-O composition of crude oil, SARA-analysis, GC-MS, and viscosity of heavy oil samples before and after the CO_2-assisted catalytic hydrothermal treatment of heavy oil sample.

2.2.1. Gas Composition of the Products

The composition of the gasses evolved after catalytic and non-catalytic hydrogenation of carbon dioxide during steam treatment, are presented in Table 2. The share of methane after CO_2 hydrogenation in the absence of the catalyst was 0.96 wt.%, which is two times more than the content of methane evolved after using Na-Fe_3O_4. This implies that the application of the catalyst suppressed the formation of methane gas and increased the selectivity toward C2–C8 normal alkanes (from 3.76% to 4.39%). Wen et al. also employed the Na-Fe3O4 catalyst in the conversion of CO_2 into aromatics. The authors implied that the selectivity of C2–C8 ranged between 2.4–3.6%, which is in accordance with the results we obtained [51].

Table 2. The Gas Composition of the experimental products.

Gas Composition, wt.%	Samples	
	HTT	**HTT + Na-Fe_3O_4**
CH_4	0.96	0.42
C2-C8	3.76	4.39
H_2	1.71	0.39
O_2	5.45	1.74
N_2	31.20	39.28
H_2S	13.78	16.05
Other gasses	43.16	37.73
Total	100	100

Moreover, the decrease in the relative content of H_2 in contrast to the blank sample (from 1.71 wt.% to 0.39 wt.%) can be related to the intensification of CO_2 hydrogenation reactions by involving a significant part of H_2 gas. The catalyst promoted hydrodesulfurization of heavy crude oil compared with the blank sample, the gaseous products of which contributed to the increase of relative content of H_2S from 13.78 to 16.05 wt.%. Moreover, the hydrodenitrogenation of heavy oil increased the content of N_2 in the gas products from 31.2 wt.% to 39.28 wt.%.

2.2.2. Group Composition of Crude Oil Samples

The group composition analysis of crude oil samples revealed significant changes, mainly in the content of resins and aromatics (Figure 6). The CO_2-assisted HydroThermal Treatment (HTT) without catalyst reduced the number of resins from 32 wt.% to 28 wt.%. Although the destruction products of resins partially increased the content of aromatics, the amount of asphaltenes has been increased from 6 wt.% to 8 wt.%. This is explained by the polymerization of the hydrocracked peripheral radicals from the aromatic rings of resins in the absence or lack of hydrogen ions. On the other hand, the Na-Fe_3O_4 contributed to the intensification of aquathermolysis reactions in the CO_2 medium such that the content of resins was reduced almost two times in contrast to the initial crude oil sample. From Figure 6, it is obvious that the destructive hydrogenation of high molecular resins produced

more light aromatic hydrocarbons raising their content by 50% (from 32.5 wt.% to 49 wt.%) as the content of asphaltenes were almost unchanged (the content of asphaltenes for initial crude oil sample and after catalytic treatment were 6.2 wt.% and 5.6 wt.%, respectively). This indicates the role of the catalyst in inhibiting the polymerization reactions, most probably because of the accelerating dehydrogenation of water and hydrogen donor species. The changes observed in the group distribution of the catalytic conversion products of CO_2 over Na-Fe_3O_4 are similar to the results reported in [52]. Many authors imply that the contents of resins and asphaltenes determine the viscosity of heavy oil and natural bitumen [53–55]. Therefore, the results of SARA analysis have to be in accordance with viscosity measurements, which are presented in the following sections. The composition of the saturated and aromatics was further studied in detail by gas chromatography-mass spectroscopy analysis method.

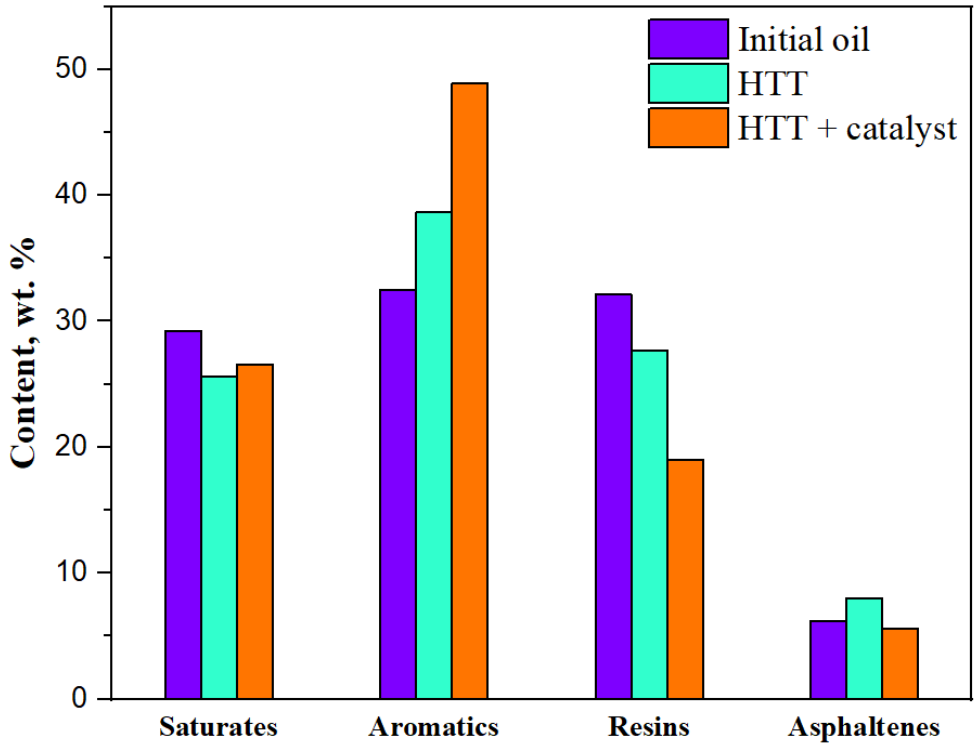

Figure 6. The group composition of oil samples.

2.2.3. Viscosity of Heavy Oil before and after CO_2 Hydrogenation

Figure 7 illustrates the results of viscosity measurements before and after hydrothermal upgrading using CO_2 in the absence and presence of the nanoparticles. All samples showed non-Newtonian behavior, and therefore the results were presented as the function of low shear rate values. The non-catalytic CO_2-assisted hydrothermal upgrading increased the viscosity values in the whole low shear rate range. This can be explained by the polymerization of hydrocracked radicals during non-catalytic HTT, which can be observed from the SARA-analysis results, particularly the increase in the content of asphaltenes (Figure 6). On the other hand, the catalytic CO_2-assisted hydrothermal upgrading of heavy oil significantly decreased the viscosity of initial crude oil from 3100 mPa·s to 2144 mPa·s. Although the obtained reduced viscosity values do not approach the viscosity of conventional crude oil resources and do not meet the requirements of downstream technological processes, the optimization of the catalyst concentration, as well as the temperature and pressure of steam in the future, can further reduce the viscosity of heavy oil.

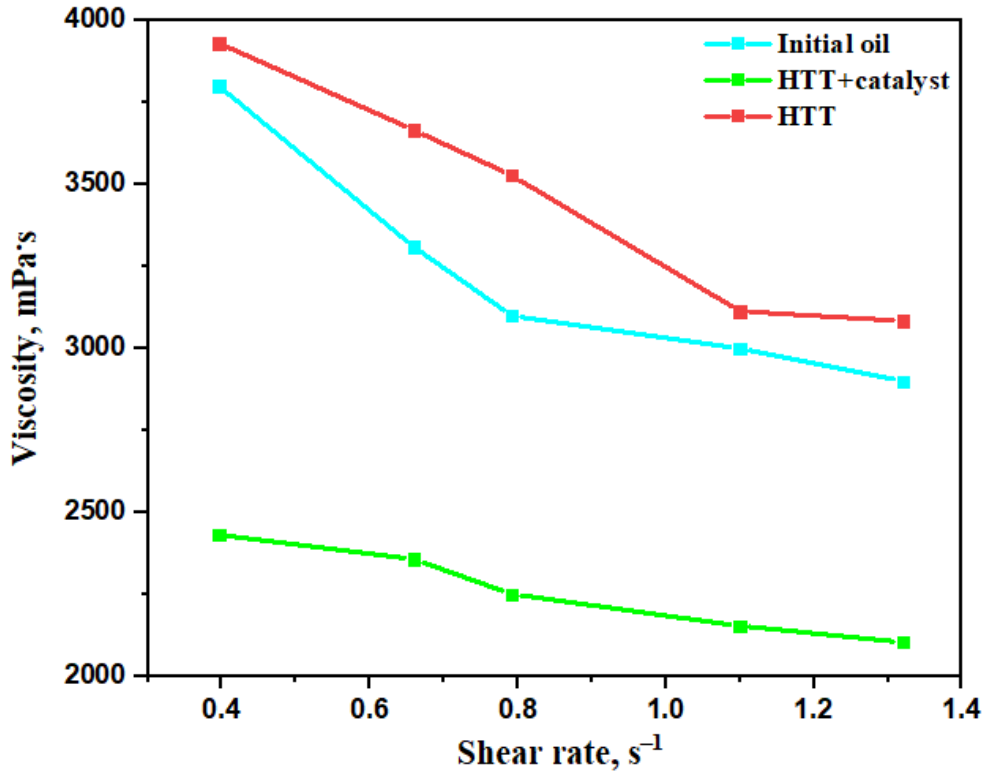

Figure 7. The shear rate-dependent viscosity values for initial and upgraded heavy oil samples.

2.2.4. Elemental Composition of Oil Samples

It was useful to investigate the elemental composition (Table 3) of crude oil samples before and after CO_2-assisted hydrothermal treatment in the absence and presence of the synthesized catalyst nanoparticles. The content of carbon was decreased, while the hydrogen content was increased essentially in the presence of the catalyst, which supports the destructive hydrogenation of high-molecular resins and asphaltenes in the composition of crude oil. The H/C ratio in the presence of the catalyst was increased by 30% in contrast to the H/C ratio of the initial crude oil sample. Although the catalyst shows less activity in the hydrodesulfurization of crude oil, the content of nitrogen and oxygen heteroatoms was significantly reduced after catalytic CO_2-assisted hydrothermal upgrading.

Table 3. Elemental composition of heavy oil samples.

Sample	Elemental Composition, %					
	C	H	N	S	O	H/C
Initial crude oil	79.01	8.74	0.45	4.85	5.85	1.32
HTT	82.11	11.30	0.00	4.71	1.88	1.64
HTT + catalyst	82.42	12.01	0.03	4.60	0.94	1.74

2.2.5. Structural Characterization of Oil Samples Using FT-IR and EPR Spectra before and after Upgrading of Heavy Oil

The FT-IR spectroscopy of heavy oil samples gives information about the structural changes in the composition of hydrocarbons by evaluating the changes in the functional groups after CO_2-assisted hydrothermal treatment in the absence and presence of the catalyst. The FT-IR spectra of oil samples before and after CO_2-assisted hydrothermal upgrading are presented in Figure 8. The spectral coefficients were estimated to quantitatively analyze the structural changes, which are summarized in Table 4.

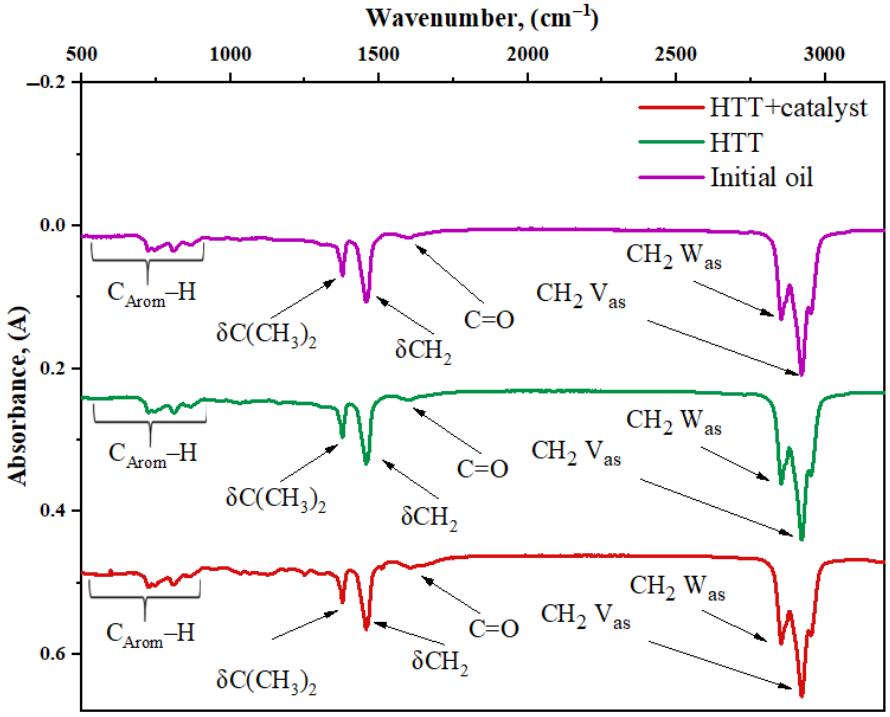

Figure 8. FT-IR spectroscopy of oil samples.

Table 4. The FT-IR spectral coefficients of crude oil samples.

Properties	Coefficients	Samples		
		Initial oil	HTT	HTT + Catalyst
Aromaticity	C_1	0.86	0.88	0.84
Branching	C_3	0.98	0.96	0.98
Aliphaticity	C_4	2.52	2.44	2.52
Sulfurization	C_5	0.86	0.89	0.88

The role of the catalyst was manifested in the comparison of spectral coefficients of oil samples after CO_2-assisted hydrothermal treatment in the absence and presence of the catalyst. A slight decrease (from 0.88 to 0.84) in aromaticity coefficient (C1) is observed after the addition of the catalyst to the reaction medium. Aliphatic coefficient (C4) significantly increases from 2.44 to 2.52, supporting the destructive hydrogenation of aromatic rings. The changes in the branching coefficient (C3) indicate the isomerization reactions during the process. Insignificant reduction in the sulfurization coefficient (C5) specifies that S=O functional groups are less involved in hydrodesulfurization reactions, which were concluded from the content of evolved H_2S gas (see Table 2) and the results of elemental composition (see Table 3) of oil sample after catalytic hydrothermal treatment.

The destructive hydrogenation reactions are mainly carried out in the resins and asphaltenes compositions, which are characterized by the concentration of paramagnetic molecules. As a rule of thumb, the paramagnetism of asphaltenes fragments is because of vanadyl complexes and unpaired electrons delocalized on polyaromatic fragments of resins and asphaltenes—Free stable Radicals (FR) [56]. The content of paramagnetic centers in the composition of asphaltenes varies between 1019–1020 sp./g. The concentration of paramagnetic centers in crude oil generally refers to the aromaticity and polymerization of the system, representing asphaltene molecules as a polybonding system that contributes to the stabilization of unpaired electrons. The EPR—spectral analysis was employed to reveal the structural changes, particularly to compare the formation of free radicals in the composition of crude oil under the influence of CO_2-assisted catalytic hydrothermal

treatment. In Figure 9, we present the signals of free radicals corresponding to the initial crude oil sample and oil samples after CO_2-assisted hydrothermal treatment in the absence and presence of the catalyst. In Figure 10, the relative intensities of free radical lines are compared. The hydrothermal upgrading without the catalyst leads to the formation of free, stable radicals. The relative intensity of free radical generation was higher with the addition of the catalyst nanoparticles because of the intensive destruction of radical fragments from the polyaromatic hydrocarbons.

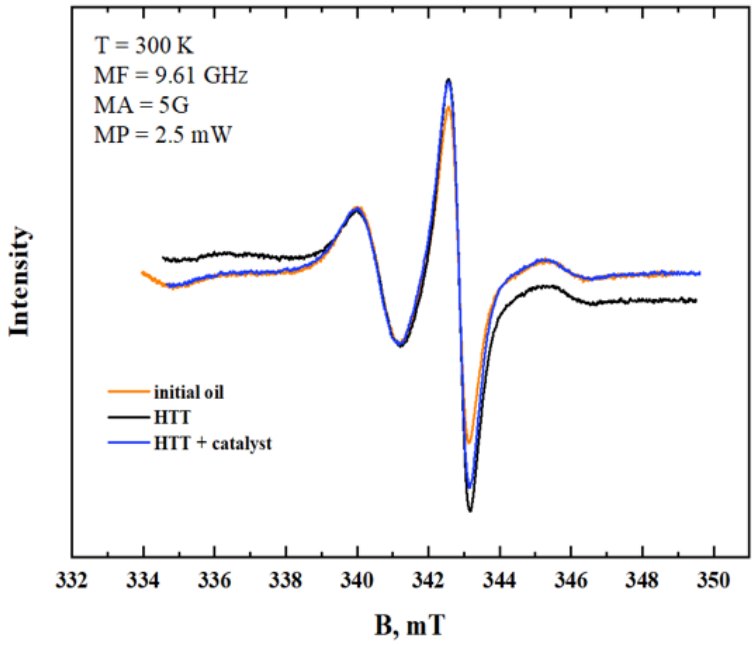

Figure 9. EPR spectra of free radicals in the composition of initial oil sample and after hydrothermal treatment in the absence and presence of the catalyst.

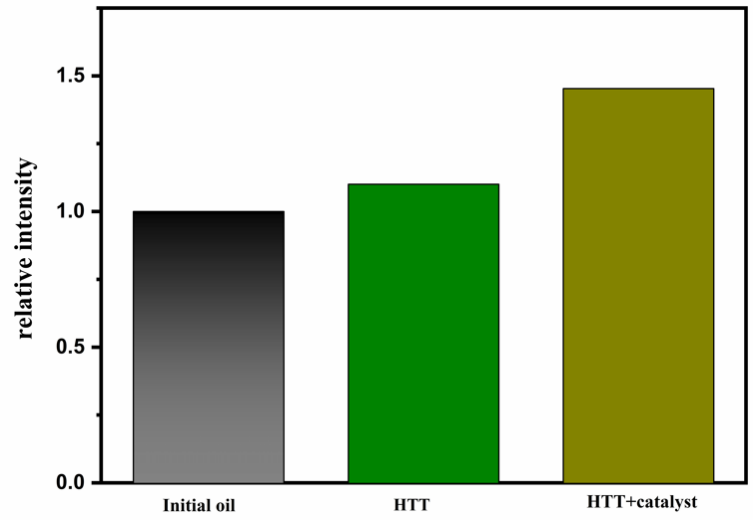

Figure 10. Relative intensities of free radicals.

2.2.6. The GC-MS Results of Saturated and Aromatics Fractions of Oil Samples

The detailed composition of isolated light fractions of heavy oil samples was investigated using the GC-MS analysis method (Figures 11–13). In Figure 11, the saturated fractions isolated from crude oil samples are evaluated by m/z = 57 ions. The results show the changes in the composition of normal alkanes toward the increasing of C14–C17 *n*-alkanes after catalytic hydrogenation of carbon dioxide. In addition, the high-molecular

normal alkanes were reduced to low-molecular *n*-alkanes. In general, the content of alkanes has been reduced a little after CO_2-assisted hydrothermal treatment without a catalyst, probably due to the polymerization of linear hydrocarbons. However, the addition of the catalyst to the reaction medium leads to the increase of the relative alkane content from 51% to 57%. The relative amount of hopanes and pregnanes decreased from 28.98% and 1.69% to 21.16% and 1.28%, respectively. Hopanes and pregnanes are high-molecular polycyclic alkanes, which are considered the most thermally stable compounds in saturated hydrocarbon fractions of crude oil. A decrease in the relative content of such compounds can be related to the destruction of the high-molecular components of crude oil.

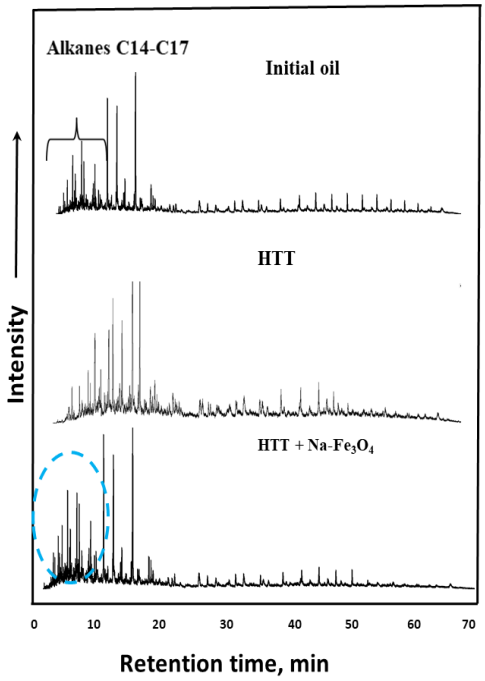

Figure 11. GC-MS spectra of saturated hydrocarbons by $m/z = 57$.

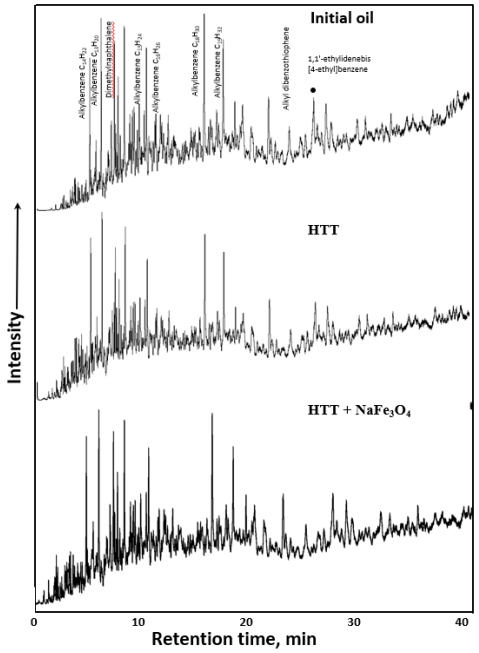

Figure 12. GC-MS of aromatics.

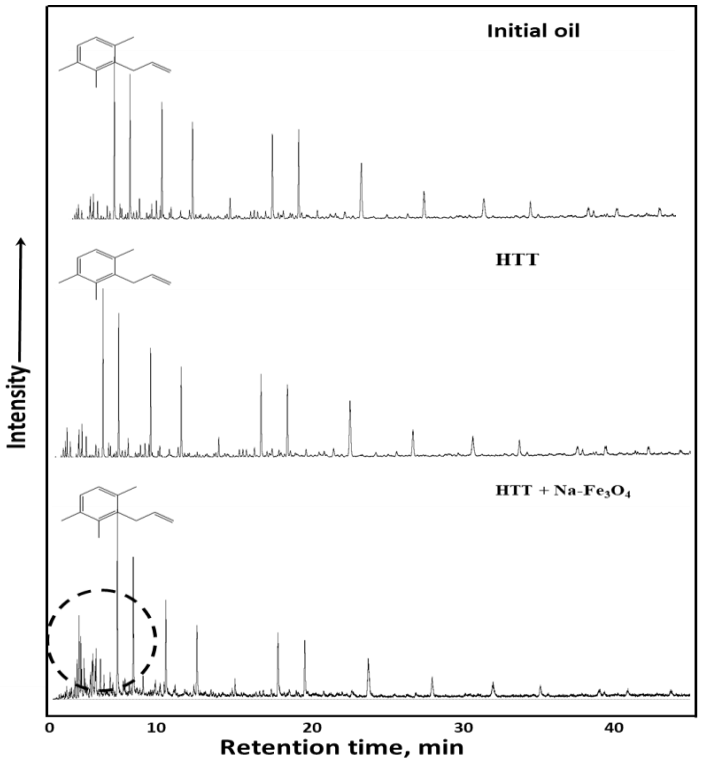

Figure 13. GC-MS spectra of 1,3,4-tri-methyl-2-alkyl-benzenes in the composition of aromatics by m/z = 134.

The results of SARA analysis showed that significant changes were in the content of aromatics (Figure 6). It was proposed that the increase in the content of aromatics was due to the detached alkyl radicals from the resins and asphaltenes. Therefore, in order to support the proposal, we have analyzed the fractions of aromatics by GC-MS (Figure 12), particularly by m/z = 134 (tri-methyl-alkyl-benzene) ion (Figure 13). The relative content of alkyl benzenes in aromatics fraction was decreased after CO_2-assisted hydrothermal treatment of oil without catalyst from 29% to 13%. However, the catalyst accelerated the destructive reactions of resins and asphaltenes, the products of which increased the number of alkyl-benzenes in the composition of aromatics from 13% to 38%. The share of heteroatom-containing compounds such as di-phenyl-sulfides, which were initially 3.69%, increased to 5.16%.

From Figure 13, one can observe an obvious increase in the intensity of peaks in the case of Na-Fe_3O_4. The comparison of the estimated total area under the peaks revealed an increase in the relative content of alkyl benzenes in aromatics fraction after CO_2-assisted hydrothermal treatment of oil from 13% to 38%. Thus, changes in the group and hydrocarbon composition of the products of catalytic CO_2-assisted aquathermolysis of heavy oil confirm the most intensive processes of destructive hydrogenation of its high-molecular components by the formation of low-molecular aliphatic and aromatic hydrocarbons at a temperature of 250 °C.

3. Materials and Methods

3.1. Synthesis of Na-Fe_3O_4 Nanoparticles

Hexahydrate of iron (III) chloride ($FeCl_3 \cdot 6H_2O$) with a mass of 2.339 g and ferrous sulfate heptahydrate ($FeSO_4 \cdot 7H_2O$) with a mass of 1.2 g were dissolved in 50 mL of distilled water. At the same time, 0.5 g of polyacrylic acid was mixed with 4.84 g of NH_4OH in 44 mL of distilled water at room temperature. After the complete dissolution of both samples, the solution containing iron metal salts was added dropwise to the second solution at room temperature and stirred for one hour. After the formation of iron oxide (Fe_3O_4) particles,

it was sonicated for 20 min to obtain smaller particles. Finally, iron oxide particles were washed several times with distilled water and dried at room temperature. Then, 2.31 g of Fe_3O_4 with 50 mL of 2.5 M sodium hydroxide placed in an autoclave at 180 °C for 8 h. The obtained sample was calcined for 6 h at 600 °C to remove the impurity.

$$2FeCl_3 + FeCl_2 + 8NH_4OH \rightarrow Fe_3O_4 + 8\ NH_4Cl + 4H_2O \quad (3)$$

$$4Fe_3O_4 + 4NaOH\ (t^\circ) \rightarrow 4NaFe_3O_4 + O_2 + 2H_2O \quad (4)$$

3.2. Characterization of the Obtained Catalyst

3.2.1. X-ray Diffraction (XRD) Analysis

The X-ray diffraction analysis was accomplished using Shimadzu XRD-7000S automatic powder diffractometer (Kyoto, Japan) using a nickel monochromator with a step of 0.008 nm and 3 s of exposure, in combination with a Bruker D2 PHASER (Bruker, Karlsruhe, Germany) and CuKα radiation with a wavelength of λ = 1.54060 nm.

3.2.2. Scanning Electron Microscope (SEM) and Energy-Dispersive X-ray Spectrometer (EDX) Analysis

SEM analysis was carried out on field emission scanning electron microscope «Merlin» (Carl Zeiss, Oberkochen, Germany) equipped with an Energy-Dispersive X-ray spectrometer (EDX mapping) «Aztec X-Max» (Oxford Instruments, London, England) to study the morphology and elemental composition of catalyst particles. Samples were coated with Au/Pd using a Quorum Q150 ES vacuum device (Quorum Technologies Ltd., East Sussex, England) in order to provide conductivity. The thickness of the cover was ~10 nm. For EDX analysis, the accelerating voltage was 20 kEv, prone current 1 nA.

3.3. The Activity of the Synthesized Catalyst Nanoparticles

3.3.1. Heavy Oil Catalytic Upgrading Experiments

The hydrothermal upgrading of heavy oil samples in the absence and presence of the synthesized catalysts was carried out in a stainless HPHT batch reactor with a stirrer manufactured by Parr Instruments (Company, Moline, IL, USA), the schematics of which are illustrated in Figure 14. The system was composed of 70 g heavy oil and 30 g water in non-catalytic experiments. Besides, for the catalytic experiments, 1.4 g of Na-Fe_3O_4 was loaded into the reaction medium. The desired pressure was supplied by injecting CO_2 after 20 min of purging to replace the trapped air from the reactor. The reactor was heated from room temperature up to 250 °C and was kept for 48 h. The initially given pressure was 10 bar, while the achieved working pressure at a temperature of 250 °C was above 90 bar.

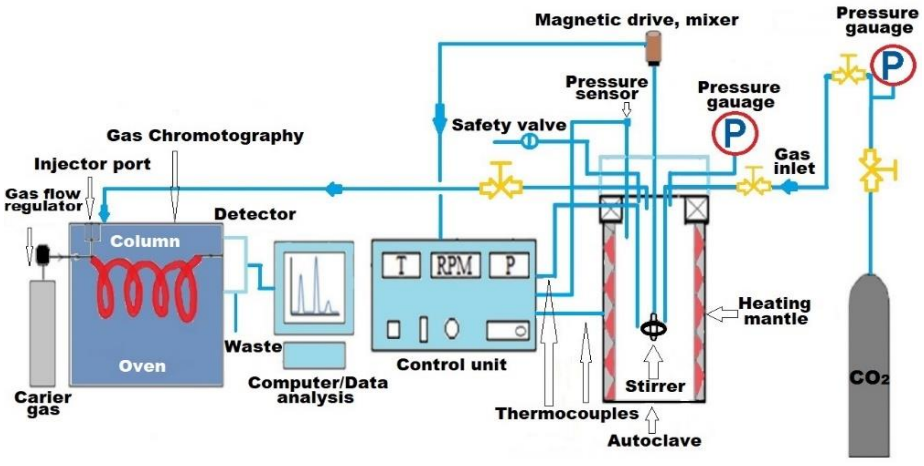

Figure 14. The schematic illustration of High Pressure-High Temperature reactor.

3.3.2. Gas Chromatography (GC) of the Evolved Gasses

The composition of the gaseous products after non-catalytic and catalytic CO_2-assisted hydrothermal upgrading was analyzed by a gas chromatography Chromatec Crystall 5000.2 (Yoshkarala, Russia), which was coupled with the HPHT reactor through specially designed tubing. The gas samples were carried along a capillary column with a length of 100 m and two absorption chambers by a continuous flow of inert Helium and Argon gasses. The temperature mode was set as follows: 90 °C for 4 min, from 90 °C to 250 °C with a heating rate of 10 °C/min. The stream velocity was 2.5 mL/min. The measurement procedures were carried out according to the ASTM D5134-98 (2008) standard. The obtained spectra were processed using the software application of Chromatec Analytics 3.0 in order to make a quantitative analysis, particularly to obtain the relative volumetric content of each gas composition. Furthermore, the Mendeley–Clapeyron equation was employed to convert a volumetric percentage of each gas component into the weight percent. The gaseous products are assumed as an ideal gas, and therefore the compressibility factor was 1. The total volume of gasses was estimated from the difference of the volumes of the empty reactor and filled with liquid (water and oil).

3.3.3. SARA-Analysis

The assessment of the group composition of heavy oil was carried out by Saturates, Aromatics, Resins, and Asphaltenes (SARA)—analysis method by dividing the crude oil composition roughly into four groups as per ASTM D4124. In this study, the precipitation of asphaltenes from crude oil was done by dissolving the oil sample in *n*-hexane. The asphaltenes, as the most polar component of heavy oil, do not dissolve in a nonpolar solvent such as *n*-hexane following the rule of "like" dissolves "like", and thus precipitate totally after 12 h. Then, the precipitates are filtered, and the residue of asphaltene fragments from the filter is extracted in a soxhlet by warm polar solvent—toluene. In its turn, the filtrates were separated in a special chromatography column filled with the neutral adsorbent—Al_2O_3 into saturated hydrocarbons, aromatics, and resins by using diluent solvents with different polarity.

3.3.4. Elemental Analysis

The elemental (CHNS-O) composition of the initial heavy oil sample and products of catalytic and non-catalytic hydrogenation of carbon dioxide were analyzed in Perkin Elmer 2400 Series II (Perkin Elmer, Waltham, MA, USA). This analysis provides information about the content of carbon, hydrogen, nitrogen, oxygen, and sulfur. Thus, the H/C ratio for each heavy oil sample is also estimated based on the results of elemental analysis.

3.3.5. Fourier Transform Infrared (FT-IR) Spectral Analysis

The FTIR spectral analysis method was employed to investigate the structural composition of initial heavy crude oil samples and the products of CO_2-assisted hydrothermal upgrading in the absence and presence of the catalyst. Moreover, this method was applied to show the end product of the synthesized catalyst and magnetite as an intermediate product. The spectra were recorded using Spectrum two Perkin Elmer (Perkin Elmer) with Single Reflection Diamond in the ranges of 4000 to 450 cm^{-1} with a resolution of 4 cm^{-1}. The following spectral coefficients—C_1, C_3, C_4, and C_5 were introduced to reveal the changes in the functional groups in the composition of crude oil systems. C_1 stands for aromaticity of heavy oil, which is defined as the ratio of optical density at the maximum of D_{1600} to D_{720}. $C_3 = D_{1380}/D_{1465}$ and $C_4 = (D_{720} + D_{1380})/D_{1600}$ characterize branching and paraffinicity, respectively; $C_5 = D_{1030}/D_{1465}$ stands for sulfurization index.

3.3.6. Viscosity Measurements

The viscosity of the initial heavy oil sample and after upgrading in the absence and presence of the catalyst was evaluated by using the rotational viscometer Fungilab Alpha L (Valencia, Spain). The measurement was carried out under constant temperature, which

was supplied by a thermostat from the Huber manufacturer. A TL5 spindle was used for the measurement of all samples, which required 6.7 mL of heavy oil sample. For each shear rate, the acceptable viscosity value was when the percentage value of the curvature of the spring in relation to the same base scale was more than 50%, and the value was constant.

3.3.7. EPR Spectral Analysis

The EPR spectra of the samples were investigated by Bruker stationary EPR spectrometer ESP-300 (Bruker, Ettlingen, Germany) with operating frequency of 9.4–9.9 GHz, X-band. The range of magnetic fields was 20–1600 mT, and the field measurement accuracy was no less than 0.01 mT. The signal detection technique uses the so-called double magnetic field modulation; in our case, the magnetic field modulation amplitude varied from 0.2 to 0.5 mT, and the magnetic field modulation frequency was 100 kHz. The concentration of paramagnetic centers was calculated using a Bruker double resonator ER4105DR. In this case, the spectra's integral intensities of the studied sample and the reference sample with a known concentration (DPPH and Mn in MgO) were compared. In the case of high-temperature EPR studies, heating was carried out using a high-temperature resonator Bruker ER4114HT, which includes a flowing nitrogen cryostat and an Oxford Instruments temperature control system. The temperature dependences of the EPR spectra were obtained in the temperature range of (293–780) K, with a step of (8–15) K, a heating rate of 2 degrees per minute, and an accuracy of not less than 2 degrees. In order to correctly record the EPR spectra of each type of paramagnetic center, in particular, in order to avoid the saturation effect, optimal microwave power values were chosen for each experiment. So, in the case of the study of free radicals (FR), which have a large saturation effect, the value of microwave power was chosen as 25 μW. The relative intensities of the spectra were estimated under the same experimental conditions, which were selected as optimal for each specific experiment.

3.3.8. Gas Chromatography-Mass Spectroscopy (GC-MS) Analysis

The fractions of saturated and aromatic compounds were studied using a gas chromatography-mass spectrometry system, including a Chromatec-Crystal 5000 gas chromatograph (Chromatec, Yoshkarala, Russia) with an ISQ mass-selective detector (Waltham, MA, USA). The Excalibur program was employed to process the results. The capillary column of GC has a length of 30 m and a diameter of 0.25 mm. The velocity of the carrier gas (Helium) was 1 mL/min. The injector temperature was 310 °C. The preset temperature program of the thermostat was as follows: temperature increases from 100 to 150 °C at a speed of 3 °C/min and from 150 to 300 °C at a speed of 12 °C/min, followed by its isotherm until the end of the analysis. The electron energy of the mass detector is 70 eV; the ion source temperature is 250 °C. The compounds were identified from the electronic library of the NIST spectra database and from literary sources.

4. Conclusions

In this study, the synthesis of Na-Fe_3O_4 nanoparticles and their characterization are discussed. Moreover, the application of Na-Fe_3O_4 in the catalysis of carbon dioxide hydrogenation and hydrothermal upgrading of heavy oil in reservoir conditions proved its activity by:

- Increasing the content of aromatics from 32.5 wt.% to 49 wt.% and reducing the content of resins from 32 wt.% to 18 wt.%, indicating the destructive hydrogenation of high-molecular compounds in the composition of crude oil.
- Reducing the viscosity of heavy oil samples from 3250 mPa·s to 2250 mPa·s and increasing H/C from 1.32 to 1.74.
- Increasing the relative intensity of free, stable radicals in the oil structure by 75%.
- Increase in the content of low-molecular *n*-alkanes (C14 –C17) and relative content of C2–C8 gaseous products from 3.76 to 4.39 wt.%.
- Increase in the relative content of alkyl benzenes in aromatics fraction after CO_2-assisted hydrothermal treatment of oil from 13% to 38%

The obtained results make Na-Fe_3O_4 nanoparticles an efficient catalyst to promote the utilization of carbon dioxide and a promising strategy for heavy oil recovery. Further work on the in-situ catalytic hydrogenation of carbon dioxide needs to be carried out to establish the optimum reservoir conditions and catalyst composition to better the quality of upgraded oil and to unlock the future green energy supply.

Author Contributions: Conceptualization, F.A. and A.V.; methodology, F.A. and T.K.; validation, N.N.; resources, O.S.; investigation, T.K. and O.M.; data curation, A.T. and N.M.; writing—original draft preparation, F.A.; writing—review and editing, F.A., A.T. and T.K.; visualization, A.T. and N.N.; supervision, A.V. and N.M. All authors have read and agreed to the published version of the manuscript.

Funding: This paper has been supported by the Kazan Federal University Strategic Academic Leadership Program (PRIORITY-2030).

Data Availability Statement: Not applicable.

Acknowledgments: Not applicable.

Conflicts of Interest: The authors declare no conflict of interest.

References

1. Lee, T.; Jang, S.-H.; Jung, S.; Kim, S.; Park, Y.-K.; Moon, D.H.; Kwon, E.E. CO_2 effects on catalytic pyrolysis of yard trimming over concrete waste. *Chem. Eng. J.* **2020**, *396*, 125331. [CrossRef]
2. Bhowmik, D. Global Carbon di Oxide Emissions in Hamilton Filter Model. *Int. J. Environ. Agric. Biotechnol.* **2020**, *5*, 1250–1258. [CrossRef]
3. Wang, Y.; Chen, E.; Tang, J. Insight on Reaction Pathways of Photocatalytic CO_2 Conversion. *ACS Catal.* **2022**, *12*, 7300–7316. [CrossRef] [PubMed]
4. Kar, S.; Kothandaraman, J.; Goeppert, A.; Prakash, G.S. Advances in catalytic homogeneous hydrogenation of carbon dioxide to methanol. *J. CO2 Util.* **2018**, *23*, 212–218. [CrossRef]
5. Kangvansura, P.; Chew, L.M.; Saengsui, W.; Santawaja, P.; Poo-Arporn, Y.; Muhler, M.; Schulz, H.; Worayingyong, A. Product distribution of CO_2 hydrogenation by K- and Mn-promoted Fe catalysts supported on N -functionalized carbon nanotubes. *Catal. Today* **2016**, *275*, 59–65. [CrossRef]
6. Galadima, A.; Muraza, O. Catalytic thermal conversion of CO_2 into fuels: Perspective and challenges. *Renew. Sustain. Energy Rev.* **2019**, *115*, 109333. [CrossRef]
7. Quitian, A.; Fernández, Y.; Ancheyta, J. Viscosity Reduction of Heavy Oil during Slurry-Phase Hydrocracking. *Chem. Eng. Technol.* **2019**, *42*, 148–155. [CrossRef]
8. Alotaibi, F.M.; González-Cortés, S.; Alotibi, M.F.; Xiao, T.; Al-Megren, H.; Yang, G.; Edwards, P.P. Enhancing the production of light olefins from heavy crude oils: Turning challenges into opportunities. *Catal. Today* **2018**, *317*, 86–98. [CrossRef]
9. Shafiei, A.; Dusseault, M.B. Geomechanics of thermal viscous oil production in sandstones. *J. Pet. Sci. Eng.* **2013**, *103*, 121–139. [CrossRef]
10. Butler, R. Some Recent Developments in SAGD. *J. Can. Pet. Technol.* **2001**, *40*, 18–22. [CrossRef]
11. Muradov, N. How to produce hydrogen from fossil fuels without CO_2 emission. *Int. J. Hydrogen Energy* **1993**, *18*, 211–215. [CrossRef]
12. Liu, Y.; Fan, H. The Effect of Hydrogen Donor Additive on the Viscosity of Heavy Oil during Steam Stimulation. *Energy Fuels* **2002**, *16*, 842–846. [CrossRef]
13. Aliev, F.; Mirzaev, O.; Kholmurodov, T.; Slavkina, O.; Vakhin, A. Utilization of Carbon Dioxide via Catalytic Hydrogenation Processes during Steam-Based Enhanced Oil Recovery. *Processes* **2022**, *10*, 2306. [CrossRef]
14. Pratama, R.A.; Babadagli, T. A review of the mechanics of heavy-oil recovery by steam injection with chemical additives. *J. Pet. Sci. Eng.* **2022**, *208*, 109717. [CrossRef]
15. Zhou, X.; Li, X.; Shen, D.; Shi, L.; Zhang, Z.; Sun, X.; Jiang, Q. CO_2 huff-n-puff process to enhance heavy oil recovery and CO_2 storage: An integration study. *Energy* **2022**, *239*, 122003. [CrossRef]
16. Orr Jr, F.M.; Taber, J.J. Use of Carbon Dioxide in Enhanced Oil Recovery. *Science* **1984**, *224*, 563–569. [CrossRef]
17. Jha, K.N. A Laboratory Study of Heavy Oil Recovery with Carbon Dioxide. *J. Can. Pet. Technol.* **1986**, *25*, 54–63. [CrossRef]
18. Vogt, C.; Groeneveld, E.; Kamsma, G.; Nachtegaal, M.; Lu, L.; Kiely, C.J.; Berben, P.H.; Meirer, F.; Weckhuysen, B.M. Unravelling structure sensitivity in CO_2 hydrogenation over nickel. *Nat. Catal.* **2018**, *1*, 127–134. [CrossRef]
19. Minh, D.P.; Roger, A.-C.; Parkhomenko, K.; L'Hospital, V.; de Vasconcelos, B.R.; Ro, K.; Mahajan, D.; Chen, L.; Singh, S.; Vo, D.-V.N. Selective Hydrogenation of Carbon Dioxide into Methanol. In *Conversion of Carbon Dioxide into Hydrocarbons Vol. 2 Technology*; Springer: Cham, Switzerland, 2020; pp. 111–157.

20. Li, Z.; Qu, Y.; Wang, J.; Liu, H.; Li, M.; Miao, S.; Li, C. Highly Selective Conversion of Carbon Dioxide to Aromatics over Tandem Catalysts. *Joule* **2019**, *3*, 570–583. [CrossRef]
21. Aziz, M.A.A.; Jalil, A.A.; Triwahyono, S.; Ahmad, A. CO_2 methanation over heterogeneous catalysts: Recent progress and future prospects. *Green Chem.* **2015**, *17*, 2647–2663. [CrossRef]
22. Gunasekar, G.H.; Jung, K.-D.; Yoon, S. Hydrogenation of CO_2 to Formate Using a Simple, Recyclable, and Efficient Heterogeneous Catalyst. *Inorg. Chem.* **2019**, *58*, 3717–3723. [CrossRef] [PubMed]
23. Liu, M.; Yi, Y.; Wang, L.; Guo, H.; Bogaerts, A. Hydrogenation of Carbon Dioxide to Value-Added Chemicals by Heterogeneous Catalysis and Plasma Catalysis. *Catalysts* **2019**, *9*, 275. [CrossRef]
24. Guil-López, R.; Mota, N.; Llorente, J.; Millán, E.; Pawelec, B.; Fierro, J.L.G.; Navarro, R.M. Methanol Synthesis from CO_2: A Review of the Latest Developments in Heterogeneous Catalysis. *Materials* **2019**, *12*, 3902. [CrossRef] [PubMed]
25. Khan, M.K.; Butolia, P.; Jo, H.; Irshad, M.; Han, D.; Nam, K.-W.; Kim, J. Selective Conversion of Carbon Dioxide into Liquid Hydrocarbons and Long-Chain α-Olefins over Fe-Amorphous AlO x Bifunctional Catalysts. *ACS Catal.* **2020**, *10*, 10325–10338. [CrossRef]
26. Saeidi, S.; Amin, N.A.S.; Rahimpour, M.R. Hydrogenation of CO_2 to value-added products—A review and potential future developments. *J. CO2 Util.* **2014**, *5*, 66–81. [CrossRef]
27. Fujita, S.-I.; Usui, M.; Takezawa, N. Mechanism of the Reverse Water Gas Shift Reaction over Cu/ZnO Catalyst. *J. Catal.* **1992**, *134*, 220–225. [CrossRef]
28. Zhu, M.; Wachs, I.E. Iron-Based Catalysts for the High-Temperature Water–Gas Shift (HT-WGS) Reaction: A Review. *ACS Catal.* **2016**, *6*, 722–732. [CrossRef]
29. Kung, H.H. Deactivation of methanol synthesis catalysts—A review. *Catal. Today* **1992**, *11*, 443–453. [CrossRef]
30. Lunde, P.J.; Kester, F.L. Carbon Dioxide Methanation on a Ruthenium Catalyst. *Ind. Eng. Chem. Process Des. Dev.* **1974**, *13*, 27–33. [CrossRef]
31. Sahebdelfar, S.; Takht Ravanchi, M. Carbon dioxide utilization for methane production: A thermodynamic analysis. *J. Pet. Sci. Eng.* **2015**, *134*, 14–22. [CrossRef]
32. Koschany, F.; Schlereth, D.; Hinrichsen, O. On the Kinetics of the Methanation of Carbon Dioxide on Coprecipitated NiAl (O) x. *Appl. Catal. B* **2016**, *181*, 504–516. [CrossRef]
33. Cai, M.; Wen, J.; Chu, W.; Cheng, X.; Li, Z. Methanation of carbon dioxide on Ni/ZrO2-Al2O3 catalysts: Effects of ZrO2 promoter and preparation method of novel ZrO_2-Al_2O_3 carrier. *J. Nat. Gas Chem.* **2011**, *20*, 318–324. [CrossRef]
34. Tsiotsias, A.I.; Charisiou, N.D.; Yentekakis, I.V.; Goula, M.A. Bimetallic Ni-Based Catalysts for CO_2 Methanation: A Review. *Nanomaterials* **2020**, *11*, 28. [CrossRef]
35. Tada, S.; Ochieng, O.J.; Kikuchi, R.; Haneda, T.; Kameyama, H. Promotion of CO_2 Methanation Activity and CH_4 Selectivity at Low Temperatures over $Ru/CeO_2/Al_2O_3$ Catalysts. *Int. J. Hydrog. Energy* **2014**, *39*, 10090–10100. [CrossRef]
36. Nakayama, T.; Ichikuni, N.; Sato, S.; Nozaki, F. Ni/Mgo catalyst prepared using citric acid for hydrogenation of carbon dioxide. *Appl. Catal. A Gen.* **1997**, *158*, 185–199. [CrossRef]
37. Du, G.; Lim, S.; Yang, Y.; Wang, C.; Pfefferle, L.; Haller, G.L. Methanation of carbon dioxide on Ni-incorporated MCM-41 catalysts: The influence of catalyst pretreatment and study of steady-state reaction. *J. Catal.* **2007**, *249*, 370–379. [CrossRef]
38. Wang, W.; Gong, J. Methanation of carbon dioxide: An overview. *Front. Chem. Sci. Eng.* **2011**, *5*, 2–10. [CrossRef]
39. De Smit, E.; Weckhuysen, B.M. The Renaissance of Iron-Based Fischer–Tropsch Synthesis: On the Multifaceted Catalyst Deactivation Behaviour. *Chem. Soc. Rev.* **2008**, *37*, 2758–2781. [CrossRef]
40. Evdokimenko, N.D.; Kapustin, G.I.; Tkachenko, O.P.; Kalmykov, K.B.; Kustov, A.L. Zn Doping Effect on the Performance of Fe-Based Catalysts for the Hydrogenation of CO_2 to Light Hydrocarbons. *Molecules* **2022**, *27*, 1065. [CrossRef]
41. Prasad, P.S.S.; Bae, J.W.; Jun, K.-W.; Lee, K.-W. Fischer–Tropsch Synthesis by Carbon Dioxide Hydrogenation on Fe-Based Catalysts. *Catal. Surv. Asia* **2008**, *12*, 170–183. [CrossRef]
42. Guo, L.; Sun, J.; Ge, Q.; Tsubaki, N. Recent advances in direct catalytic hydrogenation of carbon dioxide to valuable C2+ hydrocarbons. *J. Mater. Chem. A* **2018**, *6*, 23244–23262. [CrossRef]
43. Petala, A.; Panagiotopoulou, P. Methanation of CO_2 over alkali-promoted Ru/TiO2 catalysts: I. Effect of alkali additives on catalytic activity and selectivity. *Appl. Catal. B Environ.* **2018**, *224*, 919–927. [CrossRef]
44. Herranz, T.; Rojas, S.; Perez-Alonso, F.J.; Ojeda, M.; Terreros, P.; Fierro, J. Hydrogenation of carbon oxides over promoted Fe-Mn catalysts prepared by the microemulsion methodology. *Appl. Catal. A Gen.* **2006**, *311*, 66–75. [CrossRef]
45. Bukur, D.B.; Mukesh, D.; Patel, S.A. Promoter effects on precipitated iron catalysts for Fischer-Tropsch synthesis. *Ind. Eng. Chem. Res.* **1990**, *29*, 194–204. [CrossRef]
46. Dieterich, V.; Buttler, A.; Hanel, A.; Spliethoff, H.; Fendt, S. Power-to-Liquid via Synthesis of Methanol, DME or Fischer–Tropsch-Fuels: A Review. *Energy Environ. Sci.* **2020**, *13*, 3207–3252. [CrossRef]
47. Zhang, X.; Dai, B.; Zhu, A.; Gong, W.; Liu, C. The Simultaneous Activation of Methane and Carbon Dioxide to C2 Hydrocarbons under Pulse Corona Plasma over La_2O_3/γ-Al_2O_3 Catalyst. *Catal. Today* **2002**, *72*, 223–227. [CrossRef]
48. Zhang, Y.; Jacobs, G.; Sparks, D.E.; Dry, M.E.; Davis, B.H. CO and CO_2 hydrogenation study on supported cobalt Fischer–Tropsch synthesis catalysts. *Catal. Today* **2002**, *71*, 411–418. [CrossRef]
49. Wang, D.; Xie, Z.; Porosoff, M.D.; Chen, J.G. Recent advances in carbon dioxide hydrogenation to produce olefins and aromatics. *Chem* **2021**, *7*, 2277–2311. [CrossRef]

50. Choi, Y.H.; Ra, E.C.; Kim, E.H.; Kim, K.Y.; Jang, Y.J.; Kang, K.-N.; Choi, S.H.; Jang, J.-H.; Lee, J.S. Sodium-Containing Spinel Zinc Ferrite as a Catalyst Precursor for the Selective Synthesis of Liquid Hydrocarbon Fuels. *ChemSusChem* **2017**, *10*, 4764–4770. [CrossRef]
51. Wen, C.; Jiang, J.; Chiliu, C.; Tian, Z.; Xu, X.; Wu, J.; Wang, C.; Ma, L. Single-Step Selective Conversion of Carbon Dioxide to Aromatics over Na-Fe_3O_4/Hierarchical HZSM-5 Zeolite Catalyst. *Energy Fuels* **2020**, *34*, 11282–11289. [CrossRef]
52. Wei, J.; Ge, Q.; Yao, R.; Wen, Z.; Fang, C.; Guo, L.; Xu, H.; Sun, J. Directly Converting CO_2 into a Gasoline Fuel. *Nat. Commun.* **2017**, *8*, 15174. [CrossRef] [PubMed]
53. Vakhin, A.V.; Khelkhal, M.A.; Mukhamatdinov, I.I.; Mukhamatdinova, R.E.; Tajik, A.; Slavkina, O.V.; Malaniy, S.Y.; Gafurov, M.R.; Nasybullin, A.R.; Morozov, O.G. Changes in Heavy Oil Saturates and Aromatics in the Presence of Microwave Radiation and Iron-Based Nanoparticles. *Catalysts* **2022**, *12*, 514. [CrossRef]
54. Kholmurodov, T.; Aliev, F.; Mirzaev, O.; Dengaev, A.; Tajik, A.; Vakhin, A. Hydrothermal In-Reservoir Upgrading of Heavy Oil in the Presence of Non-Ionic Surfactants. *Processes* **2022**, *10*, 2176. [CrossRef]
55. Kim, C.; Yoo, C.-J.; Oh, H.-S.; Min, B.K.; Lee, U. Review of carbon dioxide utilization technologies and their potential for industrial application. *J. CO2 Util.* **2022**, *65*, 102239. [CrossRef]
56. Gafurov, M.; Volodin, M.; Rodionov, A.; Sorokina, A.; Dolomatov, M.; Petrov, A.; Vakhin, A.; Mamin, G.; Orlinskii, S. EPR study of spectra transformations of the intrinsic vanadyl-porphyrin complexes in heavy crude oils with temperature to probe the asphaltenes' aggregation. *J. Pet. Sci. Eng.* **2018**, *166*, 363–368. [CrossRef]